EUROPEAN ORGANIZATION FOR NUCLEAR RESEARCH

CERN – PPE/92 – 214
11 December 1992

TRANSVERSE ENERGY MEASUREMENTS IN PROTON – NUCLEUS INTERACTIONS AT HIGH ENERGY

HELIOS Collaboration

T.Akesson[3], S.Almehed[6], A.L.S.Angelis[20], H.Atherton[3], P.Aubry[8], H.W.Bartel[4], G.Beaudoin[8], J.M.Beaulieu[8], H.Beker[3], O.Benary[18], D.Bettoni[3,a], V.Bisi[19], I.Blevis[21], H.Boggild[3,b], W.Cleland[12], M.Clemen[12], B.Collick[12], F.Corriveau[7], S.Dagan[18], K.Dederichs[3,c], S.Dell'Uomo[13], P.Depommier[8], R.C.E.Devenish[3,d], N.DiGiacomo[5], S.DiLiberto[13], J.R.Dodd[20], B.Dolgoshein[10], A.Drees[4], H.En'yo[3], B.Erlandson[17], M.J.Esten[20], C.W.Fabjan[3], P.Fischer[4], Z.Fraenkel[21], A.Gaidot[15], F.Gibrat-Debu[15], P.Giubellino[19], P.Glassel[4], U.Goerlach[3], R.Haglund[6], L.A.Hamel[7], H.van Hecke[5], V.Hedberg[3], R.Heifetz[18], A.Holscher[4], B.Jacak[5], G.Jarlskog[6], S.Johansson[6], H.Kraner[2], V.Kroh[4], F.Lamarche[7], C.Leroy[7], D.Lissauer[2,18], G.London[15], B.Lorstad[6], A.Lounis[8], F.Martelli[19], A.Marzari-Chiesa[19], M.Masera[19], M.A.Mazzoni[3], E.Mazzucato[7], N.A.McCubbin[14], P.McGaughey[5], F.Meddi[13], U.Mjornmark[6], M.T.Muciaccia[1], S.Muraviev[9], M.Murray[12], M.Neubert[4], S.Nilsson[17], L.Olsen[2], Y.Oren[18], J.P.Pansart[15], Y.M.Park[12], A.Pfeiffer[4], F.Piuz[3], V.Polychronakos[2], G.Poulard[3], M.Price[3], D.Rahm[2], L.Ramello[19], L.Riccati[19], G.Romano[16], G.Rosa[13], L.Sandor[3], J.Schukraft[3], M.Sekimoto[3,e], B.Sellden[17], M.Seman[3,f], A.Shmeleva[9], V.Sidorov[11], S.Simone[1], Y.Sirois[7], H.Sletten[3], S.Smirnov[10], W.Sondheim[5], H.J.Specht[4], I.Stumer[2], J.W.Sunier[5], V.Tcherniatin[10], H.H.Thodberg[3], J.Thompson[12], V.Tikhomirov[9], I.Tserruya[21], G.Vasseur[15], R.Veenhof[3,g], R.Wigmans[3], P.Yepes[7]

Abstract

The results of two sets of transverse energy measurements, performed with incident proton beams of 200 and 450 GeV/c momentum on several nuclear targets, are presented. The transverse energy cross sections $d\sigma/dE_T$ are measured in a pseudorapidity range including the target fragmentation region ($-0.1 < \eta < 2.9$) for both data sets and also in a nearly complete pseudorapidity coverage ($-0.1 < \eta < 5.5$) for the data taken at 200 GeV/c incident momentum. A comparison is made of the transverse energy distributions in the target fragmentation region and in the full η region. We find that the mean value of pseudorapidity of the $dE_T/d\eta$ distributions shifts towards the target fragmentation region as the atomic mass number of the target increases or a selection of high transverse energy events is made. A parametrization based on a simple geometrical nucleon – nucleon scattering approach was found to be inadequate to describe all features of the transverse energy distributions. Finally, the VENUS model is compared with the experimental data.

To be submitted to Zeitschrift für Physik

1) University of Bari and INFN, I-70100 Bari, Italy.
2) Brookhaven National Laboratory, Upton, NY 11973, USA.
3) CERN, CH-1211 Geneva 23, Switzerland.
4) University of Heidelberg, D-6900 Heidelberg, Germany.
5) Los Alamos National Laboratory, Los Alamos, NM, USA.
6) University of Lund, S-22362, Lund, Sweden.
7) McGill University, Montreal, H3A2T8 Canada.
8) University of Montreal, Canada.
9) Lebedev Institute of Physics, SU-117924 Moscow, USSR.
10) Institute of Physics and Engineering, SU-115409 Moscow, USSR.
11) Institute of Nuclear Physics, Novosibirsk, USSR.
12) University of Pittsburgh, Pittsburgh PA 15213, USA.
13) University of Rome 'La Sapienza' and INFN, I-00185 Rome Italy.
14) Rutherford Appleton Laboratory, Didcot OX1 OQX, UK.
15) DPhPE, CEN-Saclay, F-91191 Gif-sur-Yvette, France.
16) University of Salerno and INFN I-84100 Salerno Italy.
17) University of Stockholm, S-11346 Sweden.
18) University of Tel Aviv, Ramat Aviv 9978 Israel.
19) University of Turin and INFN I-10100 Turin Italy.
20) University College, London, UK.
21) Weizmann Institute, Rehovot, Israel.

Visitors at CERN from:

a) University of Syracuse, Syracuse, NY, USA.
b) Niels Bohr Institute, Copenhagen, Denmark.
c) Ludwig-Maximilians-Universität, Munich, Germany.
d) Oxford University, UK.
e) Institute of Nuclear Study, Tokyo, Japan.
f) Slovak Academy of Sciences, Kosice, Czechoslovakia.
g) NIKHEF-H, Amsterdam, the Netherlands.

1 INTRODUCTION

The study of proton interactions in a nucleus has become of renewed interest owing to the intense experimental and theoretical activities related to the possibility of parton deconfinement and the formation of a quark – gluon plasma in nucleus – nucleus interactions [1]. Data on proton – nucleus interactions at high energy are needed for a better understanding of the interaction process and also provide useful information for the more complex nucleus – nucleus interactions.

In previous publications, the HELIOS Collaboration has presented the cross sections and pseudorapidity distributions for transverse energy production for several nuclear targets exposed to oxygen and sulfur beams at 200 GeV per nucleon [2,3]. Many features of the transverse energy distributions in nucleus – nucleus interactions were found to be explained by simple geometrical and kinematic considerations. On the other hand, an earlier result on p – Pb interactions at 200 GeV/c [4], gave an indication of rescattering in the target fragmentation region which is not part of the geometrical picture. As this p – Pb measurement was performed with a limited detector acceptance ($0.6 < \eta < 2.4$), a measurement with more complete coverage was desirable and is reported here. In addition, we can now compare the present proton – nucleus data with our earlier nucleus – nucleus data [2,3] in the same apparatus, and thus reduce systematic uncertainties.

In this article, we present a systematic study of transverse energy produced in interactions where Be, Al, Cu, W and U targets were exposed to a proton beam at 200 GeV/c incident momentum. Be, Al and W targets, as well as a high-pressure deuterium target, were also used in a proton exposure at 450 GeV/c. A brief comparison of the present data with trends observed in AA collisions is presented.

2 EXPERIMENTAL SET-UP

The layout of the HELIOS apparatus is shown in Fig. 1.

2.1 Beam and target region

The experiment was performed in the H8 beam line at the CERN SPS. The average beam intensity was about 5×10^5 protons per 2.3 second burst. Upstream of the target, a series of counters was used to define the beam and to veto upstream interactions. The 'pretrigger' was defined as a coincidence between the beam-defining telescopes and the silicon pad detector located downstream of

the target. Upstream interactions which could contaminate the data sample were shielded with an additional iron wall centred on the beam pipe. In the 200 GeV/c run, an anticoincidence was required between the pretrigger and the signal generated by particles that hit the large veto counter. This arrangement provided a data sample essentially free of upstream interactions.

For the deuterium target, D_2 gas at 343 atm was used, contained in a thin-walled steel cylinder. The cylinder had a length of 12 cm, corresponding to 1.3% of an interaction length of D_2, and was closed with 0.5 mm thick steel end-caps, representing 0.3% of an interaction length of Fe.

2.2 Calorimeter configuration

The HELIOS sampling calorimeters were used to measure the energy flow [2,3]. These calorimeters, which are composed of copper, uranium, and iron as sampling materials, cover nearly 4π in the centre-of-mass system. For the runs at 200 GeV/c, the uranium/scintillator calorimeter covering the forward hemisphere was replaced by a uranium/liquid-argon calorimeter of very fine granularity (ULAC).

The calorimeters also provided a trigger on the transverse energy flow. In this article, results from triggers covering two different pseudorapidity regions are given: the **backward** region ($-0.1 < \eta < 2.9$) and the **full** region ($-0.1 < \eta < 5.5$).

3 ANALYSIS AND YIELDS

Table 1 contains the list of targets, their thicknesses and the total number of events after selection for the two beam energies. The off-line cuts applied to the events are that (i) the total energy measured in the calorimeters should be within 4 standard deviations of the nominal beam value, and (ii) the signal in the small veto counter should be compatible with zero particles. The first cut eliminates events due to pile-up of particles resulting from two or more interactions; they amount to about 5% of the total sample. Hits in the small veto counter indicate the occurrence of an upstream interaction. We have estimated the percentage of rejection due to that cut, with respect to the whole sample, at 30% for the 450 GeV/c data, whereas it was less than a few per cent for the 200 GeV/c period, for which a large veto counter was already included in the trigger. More details are given in Ref. [5].

A certain level of contamination remains from non-target interactions, which we have measured in 'empty' target runs. A large fraction of these events have a transverse energy lower than 6 GeV. The

contribution of these ***non-target*** interactions is systematically subtracted from the ***target-in*** distribution. The contamination varies from 80% for $E_T \leq 6$ GeV to less than 1% for $E_T > 20$ GeV.

The analysis of the deuterium data required a different treatment because of the relatively high 'empty' target correction [6]. For the 'empty' target runs, the D_2 target was replaced by an identical steel cylinder, filled with air at 1 atm. In principle, the 'empty' target subtraction would be adequate to extract the D_2 cross section. However, in addition, we used the tracking system of the HELIOS apparatus [6] consisting of precision drift chambers and a Si-pad detector. This tracking capability permitted vertex reconstruction of the p − target interactions and, in particular, interactions in the steel end-cap of the target cylinder could be clearly distinguished from interactions in the gas volume. Control runs with a solid CH_2 target indicated the reliability of this procedure and provided estimates of the efficiency of this method as a function of the transverse energy. The number of events quoted in Table 1 are those remaining after vertex reconstruction.

In the analysis, the background due to the uranium radioactivity ('uranium noise') was treated as follows: the contribution of a calorimeter element which registered an absolute energy value less than twice its corresponding intrinsic uranium noise level was set at zero. These noise levels quantities were separately evaluated in calibration runs interspersed during the run. Typical values are 7 MeV for a cell in the electromagnetic part of the calorimeter and 35 MeV for a cell in the hadronic part.

4 MONTE CARLO CALCULATIONS

4.1 Description of the procedure

The effect of the finite resolution of the calorimeters was estimated with an event generator that was tuned to reproduce the energy flow of real events. This Monte Carlo procedure has been extensively used in the past [4] and was adapted for our proton − nucleus experimental conditions. Events were generated with an E_T distribution, flat in rapidity, and weighted subsequently by the measured pseudorapidity distributions of charged particles in proton − nucleus collisions. The transverse momentum of the particles was generated from an exponential distribution in p_T^2, giving a value of $< p_T > = 300$ MeV/c consistent with p − p data. As the calorimeter response was dependent on the particle composition, the events were generated with a mixture of charged particles (baryons, pions) and neutral pions. The ratio of baryons to mesons was taken to be 0.21, derived from the

measured ratio of positive to negative particles in the HELIOS external spectrometer [7]. Energy and momentum were conserved in this procedure.

The particles were tracked in the calorimeters using the GEANT package [8]. The longitudinal shape of the showers was parametrized according to Ref. [9], whereas for the lateral development a Gaussian shape with a FWHM of $\lambda/2$ ($X_0/2$) for hadronic (electromagnetic) showers was assumed.

The shower profile of a 200 GeV proton entering the central part of the ULAC has been measured and used for the calculation of the corrections to the forward transverse energy as described in Ref. [10].

4.2 Systematic uncertainties and correction to the transverse energy scale

The systematic uncertainties on the transverse energy in the backward and the full pseudorapidity regions were computed by Monte Carlo. Varying the e/π and e/mip ratios by a few per cent around their measured values yields an error on the transverse energy of 3% and 1.7% respectively [11]. Uncertainties in the transverse energy due to the lateral spread of the showers, resulting in an angular error, and the leakage of particles through the calorimeters were evaluated together to be 3.7%. The systematic error on the global calibration was estimated to be 4% [2]. The subtraction of the uranium noise introduces a systematic error of 5% on events that have less than 6 GeV of transverse energy. Finally when summing in quadrature all the systematic errors we obtain the following results: $\sigma(E_T)/E_T$ = 8% for $E_T \leq 6$ GeV and $\sigma(E_T)/E_T$ = 6.7% for $E_T > 6$ GeV.

To obtain the correction to the absolute transverse energy scale, we have generated many events of known transverse energy, and then passed them through the full analysis chain. The ratio in E_T between the generator input and the reconstructed Monte Carlo result was found to be: 1.14 ± 0.03 for the backward region and 1.12 ± 0.02 for the full η region.

The p − D data were normalized to the total cross section, for which we used σ_{tot} = 76±2 mb (p − D at 450 GeV/c) [12]. This procedure required the evaluation of the absolute trigger efficiency, which we obtained using the IRIS event generator [13], and found to be 0.77 for $E_T > 0.5$ GeV. The cross sections shown in Fig. 2 (as well as in Table 11) therefore have an additional systematic error of ±2.3 mb due to the total cross section and E_T threshold uncertainties.

5 EXPERIMENTAL RESULTS

The differential cross sections (in mb/GeV) are obtained using the formula:

$$d\sigma/dE_T = \frac{1}{\tau B}\frac{dN}{dE_T},$$

where $\tau = \rho \times N_a \times L/A \times 10^{-24}$ in mb^{-1} (ρ is the density in g/cm^3 , N_a is the Avogadro number of atoms per mole, L is the thickness of the target in cm, and A is the atomic weight in g/mole), B is the total number of protons on target determined from beam scalers, N is the number of events corrected for the target-out distribution and E_T is the corrected absolute transverse energy.

The corrected $d\sigma/dE_T$ cross section in mb/GeV is plotted against E_T for incident proton beams on targets with various atomic mass numbers at 450 GeV/c (Fig. 2) and at 200 GeV/c (Fig. 3). See Tables 2 – 14 for numerical results. For 200 GeV/c, the data are presented in the backward and full regions, whereas at 450 GeV/c only the backward η coverage was available. Each transverse energy distribution is obtained from minimum bias events and those triggered with nominal E_T thresholds of 10, 20, 30, and 40 GeV.

The transverse energy produced in the interaction grows proportionally to the size of the target nucleus. For low A targets, the maximum value of E_T is comparable with the p – p kinematical limit, whereas for high A targets (W and U) this limit is exceeded by at least a factor of two. The shape of the distributions shows a steeply falling behaviour for low A targets, but becomes much broader as A increases.

The number ν of collisions that a proton undergoes in a nucleus with A nucleons can be estimated from the total centre-of-mass energy $s(\nu)$ as a function of ν, required to match the maximum transverse energy E_T^{max} measured for a given target. For example, for $p_p = 200$ GeV/c, $s(\nu) \cong 2 m_p \nu p_p = (E_T^{max})^2$ gives an average of between 1 and 2 collisions in beryllium and aluminium targets, 3 in copper, and between 4 and 5 in tungsten and uranium. These values are consistent with those obtained from the usual definition of ν ($= A\sigma_{pp}/\sigma_{pA}$). This simple picture indicates that the more collisions a proton makes in a nucleus, the higher the transverse energy produced in the interaction.

In Fig. 3, we compare the E_T distributions measured in the full and backward η regions for four targets (Al, Cu, W, U). We see that the E_T produced in the backward region represents the larger fraction of the total E_T. The average contribution of the forward region ($\eta > 2.9$) is only 12% of the total E_T. This feature is also reflected in the $dE_T/d\eta$ distributions as a function of η, which are plotted in Fig. 4. The $dE_T/d\eta$ distributions are plotted in different E_T slices and are well fitted by Gaussian functions. The results clearly show the important production of the transverse energy in the target fragmentation and central regions compared with that in the beam fragmentation region.

In Fig. 5 the mean η and the width σ_η of the $dE_T/d\eta$ distributions are plotted for a heavy target (U) and a lighter target (Cu) as a function of the mean E_T value of the corresponding $dE_T/d\eta$ distribution. Numerical results are given in Table 15. The mean η values are smaller for U compared with those of Cu by 0.2 units of pseudorapidity, whilst the values of σ_η are larger for U than for Cu at small E_T but tend to converge at higher E_T. This confirms the large backward E_T production in nuclei with higher atomic mass number, and reveals in a clear way the backward shift of the pseudorapidity distribution when the E_T produced in the interaction increases. A significant narrowing of the distribution with E_T is noted, as has been previously observed in nucleus – nucleus interactions [10].

6 DISCUSSION AND CONCLUSION

In Fig. 6, we parametrize the experimental transverse energy distributions by a function suggested by a simple model based on the geometry of the collisions [14]. We assume that the cross section is proportional to the geometrical overlap of the nuclear density distributions of the target and the projectile. Neither surface effects nor nuclear deformations are included in the nuclear density profiles. The function has two adjustable parameters, which can be interpreted as the number of collisions at zero impact parameter and the mean nucleon – nucleon transverse energy ε_0. The same kind of parametrization was applied to nucleus – nucleus collisions in Ref. [2]. The fits are quite good for Al and Cu, but clearly deviate from the data in the low E_T region for heavy targets (W, U). The values of ε_0 needed to fit the data are larger for Al and Cu (2.0 and 1.91 respectively) than for W and U (1.37 and 1.34, respectively), and are larger than those obtained in oxygen-nucleus data at 200 GeV/A (ε_0 varying from 0.89 to 1.04). These results show that a picture based on purely geometrical arguments does not correctly describe proton – nucleus data for all targets in a consistent way. This confirms the

suggestion from our earlier measurement [4], where the simple geometrical picture also failed to describe the data.

In p−nucleus collisions, high E_T from individual nucleon−nucleon collisions has a relatively large probability, which makes the correlation between E_T and the number of collisions rather weak. In nucleus−nucleus collisions, however, the number of nucleon−nucleon collisions is sufficiently large that the contribution to the high E_T cross section of an individual high E_T nucleon−nucleon collision is relatively small. Thus nucleus−nucleus E_T distributions are dominated by the convolution of the 'high cross section' region of the nucleon−nucleon distributions, and this is why a simple geometrical picture [14] gives an acceptable description of the data.

Large transverse energy production in p−nucleus interactions was previously observed [4] and interpreted within the framework of multiple scattering models such as the 'Wounded Nucleon Model' (WNM). Such a description was shown to account approximately for the E_T-production cross section, although it does not explain the shifts in the η distributions as a function of E_T. Better agreement is obtained for the E_T distributions in the nuclear fragmentation region by including rescattering of the excitations in the nucleus [15] and the energy loss of the incident projectile in the sequence of collisions [16].

We have compared some of our results with VENUS (version 4.02), which is an event generator based on the String Model and principles of the Dual Parton Model [17]. Non-diffractive collisions between nucleons are included as well as reinteractions of decay products from string fragmentation with themselves and with spectator nucleons. Our measured pseudorapidity and transverse energy distributions are compared with the VENUS predictions in Figs. 7 and 8 for the (Cu,U) targets. The pseudorapidity distributions are normalized to the number of events in the corresponding E_T bin. There is general agreement between the data and VENUS; however the measured widths of the pseudorapidity distributions are systematically smaller than those produced by VENUS.

The simulation of the E_T distributions indicates acceptable agreement with the data over the full E_T range, covering typically 4 orders of magnitude in cross section. It should be noted that both for the measurement and the simulation, the trigger condition of at least three charged particles in the acceptance of the Si counter was applied. This requirement reduces the cross section for $E_T \leq 5$ GeV. The agreement between measurement and simulation of the pseudorapidity distributions, $dE_T/d\eta$, as a

function of pseudorapidity is also good. In particular, the height and the position of the maximum in pseudorapidity are reasonably well reproduced by the simulation. The shift towards smaller pseudorapidity and the decrease in the width of the distributions, as a function of increasing transverse energy, E_T, are also reasonably well reproduced.

To summarize, we have presented transverse energy distributions in proton – nucleus interactions at 200 and 450 GeV/c. The pseudorapidity distributions are studied at 200 GeV/c in a very wide pseudorapidity coverage, and are fairly well fitted by Gaussian distributions. The maximum of these distributions is located at lower pseudorapidities for heavy targets than for light targets. A systematic shift towards the target fragmentation region is clearly observed for high E_T events. The geometrical parametrization [14] fails to account for all the data in a consistent way, pointing to a possible dynamical origin which is missing in the purely geometrical picture. In comparison with the VENUS generator, we see a satisfactory agreement with the data, however with a possible systematic shift of the data towards lower pseudorapidities.

Acknowledgements

The HELIOS Collaboration acknowledges the dedication and excellent work of the staff of the CERN PS – SPS accelerator complex in providing proton beams of very high quality.

We thank the technical staff of CERN and of the institutes collaborating in HELIOS for their invaluable contributions.

We are grateful for the support given by the Natural Sciences and Engineering Research Council of Canada, the Institut de Recherche Fondamentale (CEA, France), the German Federal Ministry for Research and Technology, the Istituto Nazionale di Fisica Nucleare of Italy, the Science Research Council of Sweden, the Science and Engineering Research Council of the United Kingdom, the US Department of Energy, and the US – Israel Binational Science Foundation.

References

1. See the following 'Quark Matter' Proceedings: Quark Matter '83, Brookhaven, eds. T.W. Ludlam and H.E. Wegner [Nucl. Phys. A418 (1984)]; Quark Matter '84, Helsinki, ed. K. Kajantie [Lecture Notes in Physics (Springer Verlag, Heidelberg,1984), vol. 221]; Quark Matter '86, Asilomar, ed. M. Gyulassy [Nucl. Phys. A461 (1987)]; Quark Matter '87, Nordkirchen, eds. H. Satz, H.J. Specht and R. Stock [Z. Phys. C38 (1988)]; Quark Matter '88, Lenox, eds. G. Baym, P. Braun-Munzinger and S. Nagamiya [Nucl. Phys. A498 (1989)]; Quark Matter '90, Menton, eds. J.P. Blaizot, C. Gerschel, B. Pire, and A. Romana [Nucl. Phys. A595 (1991)].

2. T. Akesson et al., Z. Phys. C 38 (1988) 383.

3. T. Akesson et al., Phys. Lett. B 214 (1988) 295.

4. T. Akesson et al., Z. Phys. C38 (1988) 397.

5. A. Lounis, HELIOS note 430, Ph.D. thesis, Université de Montreal (1989), unpublished.

6. D. Bettoni, Ph.D. thesis, Syracuse University (1990), unpublished.

7. T. Akesson et al., Z. Phys. C46 (1990) 361.

8. R. Brun et al., Computer Newsl. 200 (1990) 13.

9. R.K. Bock et al., Nucl. Instrum. Methods 186 (1983)533.

10. T. Akesson et al., Nucl. Phys B353 (1991) 1.

11. T. Akesson et al., Nucl. Instrum. Methods A262 (1987)243.

12. Landolt-Bornstein, New Series I/Vol. 12b (1987) 173.

13. J.P. Pansart, CEA, DPhPE 89-04, March 1989.

14. A.D. Jackson and H. Boggild, Nucl. Phys. A470 (1987) 660.

15. G. Baym et al., Phys. Lett. B190 (1987) 29

16. S. Frankel and W. Frati, Nucl. Phys. B308 (1988) 699.

17. J.Aichelin and K. Werner, HD−TVP−91 (1991). K. Werner and P. Koch, Phys. Lett. B242 (1990) 251.

Table 1: Number of selected events for p − A

Momentum (GeV/c)	Target	Thickness (mm)	Number of events
450	D	120 at 343 atm	43839
	Be	12	19931
	Al	8	12161
	W	2	26077
	empty		1164
200	Be	20	44491
	Al	7.8	32570
	W	2	54220
	Cu	3	49278
	U	2.1	59830
	empty		23719

Table 2: $d\sigma/dE_T$ for p − Be at 200 GeV/c and $-0.1 < \eta < 2.9$

*E_T (GeV)	$d\sigma/dE_T$ (mb/GeV)	Error (mb/GeV)
0.600 E+00	0.286 E+01	**0.170 E+00
0.171 E+01	0.131 E+02	0.332 E+00
0.285 E+01	0.186 E+02	0.399 E+00
0.399 E+01	0.171 E+02	0.381 E+00
0.513 E+01	0.127 E+02	0.330 E+00
0.627 E+01	0.848 E+01	0.270 E+00
0.741 E+01	0.542 E+01	0.214 E+00
0.855 E+01	0.290 E+01	0.113 E+00
0.969 E+01	0.183 E+01	0.897 E-01
0.108 E+02	0.106 E+01	0.646 E-01
0.120 E+02	0.719 E+00	0.505 E-01
0.131 E+02	0.262 E+00	0.125 E-01
0.143 E+02	0.179 E+00	0.984 E-02
0.154 E+02	0.131 E+00	0.754 E-02
0.165 E+02	0.481 E-01	0.539 E-02
0.177 E+02	0.224 E-01	0.176 E-02
0.188 E+02	0.157 E-01	0.132 E-02
0.200 E+02	0.272 E-02	0.114 E-02
0.211 E+02	0.335 E-02	0.972 E-03

*The first column gives the transverse energy at the centre of the bin, which has a fixed width of 0.5 GeV. ** The error on the lowest E_T bin is likely to be somewhat underestimated owing to trigger threshold effects, which are difficult to evaluate.

Table 3: $d\sigma/dE_T$ for p − Al at 200 GeV/c and $-0.1 < \eta < 2.9$

*E_T (GeV)	$d\sigma/dE_T$ (mb/GeV)	Error (mb/GeV)
0.600 E+00	0.197 E+02	**0.886 E+00
0.171 E+01	0.383 E+02	0.150 E+01
0.285 E+01	0.450 E+02	0.172 E+01
0.399 E+01	0.359 E+02	0.163 E+01
0.513 E+01	0.306 E+02	0.151 E+01
0.627 E+01	0.249 E+02	0.135 E+01
0.741 E+01	0.177 E+02	0.112 E+01
0.855 E+01	0.135 E+02	0.938 E+00
0.969 E+01	0.957 E+01	0.441 E+00
0.108 E+02	0.618 E+01	0.339 E+00
0.120 E+02	0.368 E+01	0.233 E+00
0.131 E+02	0.253 E+01	0.186 E+00
0.143 E+02	0.196 E+01	0.144 E+00
0.154 E+02	0.108 E+01	0.393 E-01
0.165 E+02	0.800 E+00	0.280 E-01
0.177 E+02	0.395 E+00	0.226 E-01
0.188 E+02	0.252 E+00	0.185 E-01
0.200 E+02	0.145 E+00	0.134 E-01
0.211 E+02	0.272 E-01	0.593 E-02
0.222 E+02	0.209 E-01	0.490 E-02
0.234 E+02	0.709 E-02	0.407 E-02

*The first column gives the transverse energy at the centre of the bin, which has a fixed width of 0.5 GeV. ** The error on the lowest E_T bin is likely to be somewhat underestimated owing to trigger threshold effects, which are difficult to evaluate.

Table 4: $d\sigma/dE_T$ for p − Cu at 200 GeV/c and $-0.1 < \eta < 2.9$

*E_T (GeV)	$d\sigma/dE_T$ (mb/GeV)	Error (mb/GeV)
0.600 E+00	0.177 E+02	**0.124 E+01
0.171 E+01	0.481 E+02	0.191 E+01
0.285 E+01	0.582 E+02	0.213 E+01
0.399 E+01	0.672 E+02	0.219 E+01
0.513 E+01	0.560 E+02	0.200 E+01
0.627 E+01	0.507 E+02	0.179 E+01
0.741 E+01	0.428 E+02	0.161 E+01
0.855 E+01	0.310 E+02	0.137 E+01
0.969 E+01	0.249 E+02	0.118 E+01
0.108 E+02	0.166 E+02	0.921 E+00
0.120 E+02	0.124 E+02	0.775 E+00
0.131 E+02	0.108 E+02	0.371 E+00
0.143 E+02	0.753 E+01	0.308 E+00
0.154 E+02	0.488 E+01	0.245 E+00
0.165 E+02	0.350 E+01	0.213 E+00
0.177 E+02	0.229 E+01	0.164 E+00
0.188 E+02	0.143 E+01	0.549 E-01
0.200 E+02	0.859 E+00	0.438 E-01
0.211 E+02	0.418 E+00	0.311 E-01
0.234 E+02	0.203 E+00	0.814 E-02
0.245 E+02	0.112 E+00	0.736 E-02
0.257 E+02	0.585 E-01	0.538 E-02
0.268 E+02	0.227 E-01	0.429 E-02
0.279 E+02	0.858 E-02	0.276 E-02
0.314 E+02	0.450 E-02	0.239 E-02

*The first column gives the transverse energy at the centre of the bin, which has a fixed width of 0.5 GeV. ** The error on the lowest E_T bin is likely to be somewhat underestimated owing to trigger threshold effects, which are difficult to evaluate.

Table 5: $d\sigma/dE_T$ for p − W at 200 GeV/c and $-0.1 < \eta < 2.9$

*E_T (GeV)	$d\sigma/dE_T$ (mb/GeV)	Error (mb/GeV)
0.600 E+00	0.883 E+02	**0.116 E+02
0.170 E+01	0.151 E+03	0.120 E+02
0.400 E+01	0.150 E+03	0.676 E+01
0.510 E+01	0.133 E+03	0.623 E+01
0.630 E+01	0.108 E+03	0.532 E+01
0.740 E+01	0.106 E+03	0.517 E+01
0.850 E+01	0.884 E+02	0.449 E+01
0.970 E+01	0.681 E+02	0.382 E+01
0.108 E+02	0.538 E+02	0.340 E+01
0.120 E+02	0.460 E+02	0.314 E+01
0.131 E+02	0.417 E+02	0.280 E+01
0.154 E+02	0.237 E+02	0.211 E+01
0.177 E+02	0.170 E+02	0.562 E+00
0.188 E+02	0.128 E+02	0.496 E+00
0.199 E+02	0.958 E+01	0.425 E+00
0.211 E+02	0.701 E+01	0.372 E+00
0.222 E+02	0.567 E+01	0.318 E+00
0.234 E+02	0.412 E+01	0.277 E+00
0.245 E+02	0.308 E+01	0.234 E+00
0.256 E+02	0.187 E+01	0.594 E-01
0.268 E+02	0.151 E+01	0.536 E-01
0.279 E+02	0.105 E+01	0.445 E-01
0.302 E+02	0.397 E+00	0.881 E-02
0.314 E+02	0.269 E+00	0.748 E-02
0.325 E+02	0.198 E+00	0.634 E-02
0.336 E+02	0.118 E+00	0.481 E-02
0.348 E+02	0.775 E-01	0.406 E-02
0.359 E+02	0.573 E-01	0.343 E-02
0.371 E+02	0.409 E-01	0.287 E-02
0.382 E+02	0.231 E-01	0.242 E-02
0.393 E+02	0.114 E-01	0.130 E-02
0.404 E+02	0.886 E-02	0.118 E-02
0.416 E+02	0.633 E-02	0.146 E-02
0.428 E+02	0.502 E-02	0.956 E-03

*The first column gives the transverse energy at the centre of the bin, which has a fixed width of 0.5 GeV. ** The error on the lowest E_T bin is likely to be somewhat underestimated owing to trigger threshold effects, which are difficult to evaluate.

Table 6: $d\sigma/dE_T$ for p − U at 200 GeV/c and $-0.1 < \eta < 2.9$

*E_T (GeV)	$d\sigma/dE_T$ (mb/GeV)	Error (mb/GeV)
0.600 E+00	0.209 E+02	**0.364 E+01
0.171 E+01	0.927 E+02	0.611 E+01
0.285 E+01	0.123 E+03	0.698 E+01
0.399 E+01	0.158 E+03	0.740 E+01
0.513 E+01	0.128 E+03	0.664 E+01
0.627 E+01	0.136 E+03	0.640 E+01
0.741 E+01	0.117 E+03	0.584 E+01
0.855 E+01	0.104 E+03	0.530 E+01
0.969 E+01	0.921 E+02	0.492 E+01
0.108 E+02	0.738 E+02	0.435 E+01
0.120 E+02	0.678 E+02	0.410 E+01
0.131 E+02	0.595 E+02	0.239 E+01
0.143 E+02	0.484 E+02	0.215 E+01
0.154 E+02	0.383 E+02	0.190 E+01
0.165 E+02	0.329 E+02	0.177 E+01
0.177 E+02	0.250 E+02	0.153 E+01
0.188 E+02	0.218 E+02	0.144 E+01
0.120 E+02	0.152 E+02	0.119 E+01
0.211 E+02	0.105 E+02	0.957 E+00
0.222 E+02	0.875 E+01	0.910 E+00
0.234 E+02	0.787 E+01	0.387 E+00
0.245 E+02	0.556 E+01	0.320 E+00
0.257 E+02	0.338 E+01	0.248 E+00
0.268 E+02	0.273 E+01	0.224 E+00
0.279 E+02	0.171 E+01	0.176 E+00
0.291 E+02	0.118 E+01	0.148 E+00
0.302 E+02	0.831 E+00	0.402 E-01
0.325 E+02	0.494 E+00	0.308 E-01
0.336 E+02	0.362 E+00	0.266 E-01
0.348 E+02	0.178 E+00	0.186 E-01
0.359 E+02	0.102 E+00	0.126 E-01
0.371 E+02	0.965 E-01	0.104 E-01
0.381 E+02	0.660 E-01	0.869 E-02
0.393 E+02	0.498 E-01	0.651 E-02
0.405 E+02	0.269 E-01	0.746 E-02
0.416 E+02	0.308 E-01	0.434 E-02
0.428 E+02	0.743 E-02	0.425 E-02
0.473 E+02	0.478 E-02	0.326 E-02
0.485 E+02	0.443 E-02	0.237 E-02

*The first column gives the transverse energy at the centre of the bin, which has a fixed width of 0.5 GeV. ** The error on the lowest E_T bin is likely to be somewhat underestimated owing to trigger threshold effects, which are difficult to evaluate.

Table 7: $d\sigma/dE_T$ for p − Al at 200 GeV/c and $-0.1 < \eta < 5.5$

*E_T (GeV)	$d\sigma/dE_T$ (mb/GeV)	Error (mb/GeV)
0.840 E+01	0.296 E+02	**0.159 E+01
0.950 E+01	0.237 E+02	0.146 E+01
0.106 E+02	0.201 E+02	0.140 E+01
0.118 E+02	0.184 E+02	0.127 E+01
0.129 E+02	0.144 E+02	0.110 E+01
0.140 E+02	0.970 E+01	0.926 E+00
0.151 E+02	0.801 E+01	0.728 E+00
0.162 E+02	0.405 E+01	0.283 E+00
0.174 E+02	0.348 E+01	0.239 E+00
0.185 E+02	0.208 E+01	0.160 E+00
0.196 E+02	0.107 E+01	0.115 E+00
0.207 E+02	0.800 E+00	0.108 E+00
0.218 E+02	0.396 E+00	0.229 E-01
0.230 E+02	0.178 E+00	0.313 E-01
0.252 E+02	0.574 E-01	0.746 E-02
0.263 E+02	0.259 E-01	0.588 E-02
0.274 E+02	0.116 E-01	0.542 E-02
0.286 E+02	0.585 E-02	0.408 E-02

*The first column gives the transverse energy at the centre of the bin, which has a fixed width of 0.5 GeV. ** The error on the lowest E_T bin is likely to be somewhat underestimated owing to trigger threshold effects, which are difficult to evaluate.

Table 8: $d\sigma/dE_T$ for p − Cu at 200 GeV/c and $-0.1 < \eta < 5.5$

*E_T (GeV)	$d\sigma/dE_T$ (mb/GeV)	Error (mb/GeV)
0.600 E+00	0.192 E+01	**0.437 E+00
0.170 E+01	0.130 E+02	0.220 E+01
0.280 E+01	0.155 E+02	0.240 E+01
0.390 E+01	0.200 E+02	0.250 E+01
0.500 E+01	0.233 E+02	0.170 E+01
0.620 E+01	0.369 E+02	0.213 E+01
0.730 E+01	0.487 E+02	0.235 E+01
0.840 E+01	0.506 E+02	0.239 E+01
0.950 E+01	0.469 E+02	0.237 E+01
0.106 E+02	0.457 E+02	0.225 E+01
0.118 E+02	0.400 E+02	0.207 E+01
0.129 E+02	0.352 E+02	0.188 E+01
0.140 E+02	0.289 E+02	0.161 E+01
0.151 E+02	0.181 E+02	0.133 E+01
0.162 E+02	0.163 E+02	0.120 E+01
0.174 E+02	0.130 E+02	0.107 E+01
0.185 E+02	0.984 E+01	0.915 E+00
0.196 E+02	0.720 E+01	0.405 E+00
0.207 E+02	0.477 E+01	0.331 E+00
0.218 E+02	0.309 E+01	0.264 E+00
0.230 E+02	0.219 E+01	0.101 E+00
0.241 E+02	0.137 E+01	0.809 E-01
0.252 E+02	0.687 E+00	0.583 E-01
0.263 E+02	0.319 E+00	0.141 E-01
0.274 E+02	0.287 E+00	0.123 E-01
0.286 E+02	0.177 E+00	0.986 E-02
0.297 E+02	0.774 E-01	0.727 E-02
0.308 E+02	0.400 E-01	0.902 E-02
0.319 E+02	0.281 E-01	0.456 E-02
0.330 E+02	0.194 E-01	0.373 E-02
0.342 E+02	0.108 E-01	0.306 E-02
0.353 E+02	0.298 E-02	0.254 E-02
0.420 E+02	0.186 E-02	0.910 E-03

*The first column gives the transverse energy at the centre of the bin, which has a fixed width of 0.5 GeV. ** The error on the lowest E_T bin is likely to be somewhat underestimated owing to trigger threshold effects, which are difficult to evaluate.

Table 9: $d\sigma/dE_T$ for p − W at 200 GeV/c and $-0.1 < \eta < 5.5$

$*E_T$ (GeV)	$d\sigma/dE_T$ (mb/GeV)	Error (mb/GeV)
0.600 E+00	0.115 E+02	**0.453 E+01
0.170 E+01	0.300 E+02	0.150 E+02
0.280 E+01	0.606 E+02	0.886 E+01
0.390 E+01	0.620 E+02	0.519 E+01
0.500 E+01	0.894 E+02	0.553 E+01
0.620 E+01	0.999 E+02	0.594 E+01
0.730 E+01	0.959 E+02	0.581 E+01
0.840 E+01	0.112 E+03	0.579 E+01
0.950 E+01	0.104 E+03	0.548 E+01
0.106 E+02	0.976 E+02	0.507 E+01
0.118 E+02	0.803 E+02	0.472 E+01
0.129 E+02	0.717 E+02	0.448 E+01
0.140 E+02	0.659 E+02	0.402 E+01
0.151 E+02	0.586 E+02	0.345 E+01
0.162 E+02	0.493 E+02	0.326 E+01
0.174 E+02	0.423 E+02	0.296 E+01
0.185 E+02	0.350 E+02	0.269 E+01
0.196 E+02	0.311 E+02	0.250 E+01
0.207 E+02	0.241 E+02	0.218 E+01
0.218 E+02	0.178 E+02	0.176 E+01
0.230 E+02	0.144 E+02	0.541 E+00
0.241 E+02	0.999 E+01	0.442 E+00
0.252 E+02	0.738 E+01	0.378 E+00
0.263 E+02	0.571 E+01	0.324 E+00
0.274 E+02	0.434 E+01	0.291 E+00
0.286 E+02	0.332 E+01	0.241 E+00
0.297 E+02	0.212 E+01	0.163 E+00
0.308 E+02	0.147 E+01	0.166 E+00
0.319 E+02	0.102 E+01	0.451 E-01
0.330 E+02	0.667 E+00	0.356 E-01
0.342 E+02	0.447 E+00	0.297 E-01
0.353 E+02	0.265 E+00	0.228 E-01
0.364 E+02	0.180 E+00	0.191 E-01
0.375 E+02	0.853 E-01	0.429 E-02
0.386 E+02	0.687 E-01	0.374 E-02
0.398 E+02	0.359 E-01	0.265 E-02
0.409 E+02	0.216 E-01	0.234 E-02
0.420 E+02	0.146 E-01	0.163 E-02
0.431 E+02	0.798 E-02	0.145 E-02
0.442 E+02	0.563 E-02	0.890 E-03
0.454 E+02	0.246 E-02	0.749 E-03
0.465 E+02	0.148 E-02	0.917 E-03
0.487 E+02	0.133 E-02	0.127 E-02

*The first column gives the transverse energy at the centre of the bin, which has a fixed width of 0.5 GeV. ** The error on the lowest E_T bin is likely to be somewhat underestimated owing to trigger threshold effects, which are difficult to evaluate.

Table 10: $d\sigma/dE_T$ for p − U at 200 GeV/c and $-0.1 < \eta < 5.5$

*E_T (GeV)	$d\sigma/dE_T$ (mb/GeV)	Error (mb/GeV)
0.600 E+00	0.126 E+01	**0.754 E+00
0.170 E+01	0.363 E+01	0.855 E+00
0.280 E+01	0.938 E+01	0.166 E+01
0.390 E+01	0.235 E+02	0.222 E+01
0.500 E+01	0.506 E+02	0.315 E+01
0.620 E+01	0.828 E+02	0.407 E+01
0.730 E+01	0.102 E+03	0.481 E+01
0.840 E+01	0.127 E+03	0.529 E+01
0.950 E+01	0.121 E+03	0.519 E+01
0.106 E+02	0.105 E+03	0.504 E+01
0.118 E+02	0.111 E+03	0.482 E+01
0.129 E+02	0.101 E+03	0.458 E+01
0.140 E+02	0.861 E+02	0.408 E+01
0.151 E+02	0.812 E+02	0.369 E+01
0.162 E+02	0.717 E+02	0.346 E+01
0.174 E+02	0.600 E+02	0.316 E+01
0.185 E+02	0.594 E+02	0.192 E+01
0.196 E+02	0.459 E+02	0.167 E+01
0.207 E+02	0.361 E+02	0.144 E+01
0.218 E+02	0.295 E+02	0.125 E+01
0.230 E+02	0.223 E+02	0.107 E+01
0.241 E+02	0.172 E+02	0.935 E+00
0.252 E+02	0.160 E+02	0.891 E+00
0.263 E+02	0.102 E+02	0.614 E+00
0.274 E+02	0.944 E+01	0.278 E+00
0.286 E+02	0.652 E+01	0.183 E+00
0.297 E+02	0.494 E+01	0.163 E+00
0.308 E+02	0.295 E+01	0.933 E-01
0.319 E+02	0.208 E+01	0.816 E-01
0.330 E+02	0.134 E+01	0.851 E-01
0.342 E+02	0.111 E+01	0.235 E-01
0.353 E+02	0.852 E+00	0.188 E-01
0.364 E+02	0.610 E+00	0.156 E-01
0.375 E+02	0.381 E+00	0.129 E-01
0.386 E+02	0.262 E+00	0.116 E-01
0.398 E+02	0.181 E+00	0.104 E-01
0.409 E+02	0.122 E+00	0.994 E-02
0.420 E+02	0.595 E-01	0.865 E-02
0.431 E+02	0.385 E-01	0.422 E-02
0.442 E+02	0.199 E-01	0.502 E-02
0.454 E+02	0.105 E-01	0.525 E-02
0.465 E+02	0.878 E-02	0.339 E-02
0.510 E+02	0.617 E-02	0.398 E-02

*The first column gives the transverse energy at the centre of the bin, which has a fixed width of 0.5 GeV. ** The error on the lowest E_T bin is likely to be somewhat underestimated owing to trigger threshold effects, which are difficult to evaluate.

Table 11: $d\sigma/dE_T$ for p − D at 450 GeV/c and $-0.1 < \eta < 2.9$

*E_T (GeV)	$d\sigma/dE_T$ (mb/GeV)	Error (mb/GeV)
0.750 E+00	0.964 E+01	**0.31 E+00
0.125 E+01	0.140 E+02	0.32 E+00
0.175 E+01	0.165 E+02	0.36 E+00
0.225 E+01	0.180 E+02	0.36 E+00
0.275 E+01	0.172 E+02	0.37 E+00
0.325 E+01	0.150 E+02	0.38 E+00
0.375 E+01	0.107 E+02	0.37 E+00
0.425 E+01	0.744 E+01	0.35 E+00
0.475 E+01	0.437 E+01	0.36 E+00
0.525 E+01	0.311 E+01	0.33 E+00
0.575 E+01	0.175 E+01	0.33 E+00
0.625 E+01	0.110 E+01	0.32 E+00
0.675 E+01	0.760 E+00	0.29 E+00
0.725 E+01	0.480 E+00	0.25 E+00

*The first column gives the transverse energy at the centre of the bin, which has a fixed width of 0.5 GeV. ** The error on the lowest E_T bin is likely to be somewhat underestimated owing to trigger threshold effects, which are difficult to evaluate.

Table 12: $d\sigma/dE_T$ for p − Be at 450 GeV/c and $-0.1 < \eta < 2.9$

*E_T (GeV)	$d\sigma/dE_T$ (mb/GeV)	Error (mb/GeV)
0.600 E+00	0.997 E+01	**0.786 E+00
0.180 E+01	0.250 E+02	0.110 E+01
0.300 E+01	0.276 E+02	0.117 E+01
0.420 E+01	0.226 E+02	0.102 E+01
0.540 E+01	0.155 E+02	0.879 E+00
0.655 E+01	0.102 E+02	0.695 E+00
0.774 E+01	0.563 E+01	0.555 E+00
0.893 E+01	0.366 E+01	0.396 E+00
0.101 E+02	0.190 E+01	0.312 E+00
0.113 E+02	0.740 E+00	0.125 E+00
0.125 E+02	0.579 E+00	0.350 E-01
0.137 E+02	0.388 E+00	0.296 E-01
0.149 E+02	0.236 E+00	0.211 E-01
0.161 E+02	0.113 E+00	0.167 E-01
0.173 E+02	0.765 E-01	0.125 E-01
0.184 E+02	0.479 E-01	0.109 E-01
0.196 E+02	0.286 E-01	0.110 E-01
0.232 E+02	0.118 E-01	0.443 E-02
0.303 E+02	0.853 E-03	0.105 E-03
0.327 E+02	0.133 E-02	0.146 E-03
0.339 E+02	0.121 E-03	0.722 E-04

*The first column gives the transverse energy at the centre of the bin, which has a fixed width of 0.5 GeV. ** The error on the lowest E_T bin is likely to be somewhat underestimated owing to trigger threshold effects, which are difficult to evaluate.

Table 13: $d\sigma/dE_T$ for p − Al at 450 GeV/c and $-0.1 < \eta < 2.9$

$*E_T$ (GeV)	$d\sigma/dE_T$ (mb/GeV)	Error (mb/GeV)
0.600 E+00	0.279 E+02	**0.260 E+01
0.180 E+01	0.524 E+02	0.326 E+01
0.300 E+01	0.566 E+02	0.333 E+01
0.420 E+01	0.504 E+02	0.302 E+01
0.540 E+01	0.381 E+02	0.265 E+01
0.650 E+01	0.230 E+02	0.200 E+01
0.770 E+01	0.193 E+02	0.191 E+01
0.890 E+01	0.126 E+02	0.148 E+01
0.100 E+01	0.942 E+01	0.129 E+01
0.110 E+01	0.534 E+01	0.387 E+00
0.125 E+02	0.381 E+01	0.186 E+00
0.137 E+02	0.257 E+01	0.138 E+00
0.149 E+02	0.149 E+01	0.105 E+00
0.161 E+02	0.117 E+01	0.900 E-01
0.173 E+02	0.789 E+00	0.769 E-01
0.184 E+02	0.423 E+00	0.521 E-01
0.196 E+02	0.295 E+00	0.408 E-01
0.208 E+02	0.122 E+00	0.385 E-01
0.220 E+02	0.129 E+00	0.318 E-01
0.256 E+02	0.123 E-01	0.116 E-02
0.303 E+02	0.142 E-02	0.170 E-03
0.351 E+02	0.422 E-03	0.147 E-03

*The first column gives the transverse energy at the centre of the bin, which has a fixed width of 0.5 GeV. ** The error on the lowest E_T bin is likely to be somewhat underestimated owing to trigger threshold effects, which are difficult to evaluate.

Table 14: $d\sigma/dE_T$ for p − W at 450 GeV/c and $-0.1 < \eta < 2.9$

*E_T (GeV)	$d\sigma/dE_T$ (mb/GeV)	Error (mb/GeV)
0.600 E+00	0.794 E+02	**0.107 E+02
0.180 E+01	0.122 E+03	0.120 E+02
0.300 E+01	0.165 E+03	0.133 E+02
0.420 E+01	0.168 E+03	0.129 E+02
0.540 E+01	0.122 E+03	0.113 E+02
0.650 E+01	0.125 E+03	0.110 E+02
0.770 E+01	0.115 E+03	0.107 E+02
0.890 E+01	0.936 E+02	0.912 E+01
0.101 E+02	0.800 E+02	0.854 E+01
0.113 E+02	0.627 E+02	0.735 E+01
0.125 E+02	0.499 E+02	0.320 E+01
0.137 E+02	0.431 E+02	0.187 E+01
0.149 E+02	0.354 E+02	0.136 E+01
0.161 E+02	0.288 E+02	0.115 E+01
0.173 E+02	0.251 E+02	0.107 E+01
0.184 E+02	0.181 E+02	0.921 E+00
0.196 E+02	0.135 E+02	0.793 E+00
0.208 E+02	0.106 E+02	0.698 E+00
0.220 E+02	0.848 E+01	0.625 E+00
0.232 E+02	0.669 E+01	0.545 E+00
0.244 E+02	0.528 E+01	0.489 E+00
0.255 E+02	0.473 E+01	0.452 E+00
0.268 E+02	0.264 E+01	0.327 E+00
0.280 E+02	0.232 E+01	0.278 E+00
0.291 E+02	0.160 E+01	0.251 E+00
0.303 E+02	0.826 E+00	0.753 E-01
0.315 E+02	0.930 E+00	0.662 E-01
0.327 E+02	0.585 E+00	0.593 E-01
0.339 E+02	0.627 E+00	0.384 E-01
0.351 E+02	0.288 E+00	0.319 E-01
0.363 E+02	0.178 E+00	0.253 E-01
0.375 E+02	0.217 E+00	0.248 E-01
0.387 E+02	0.107 E+00	0.180 E-01
0.434 E+02	0.324 E-01	0.327 E-02
0.446 E+02	0.191 E-01	0.247 E-02
0.458 E+02	0.136 E-01	0.211 E-02
0.470 E+02	0.614 E-02	0.168 E-02
0.482 E+02	0.757 E-02	0.169 E-02
0.494 E+02	0.512 E-02	0.122 E-02
0.518 E+02	0.251 E-02	0.997 E-03

*The first column gives the transverse energy at the centre of the bin, which has a fixed width of 0.5 GeV. ** The error on the lowest E_T bin is likely to be somewhat underestimated owing to trigger threshold effects, which are difficult to evaluate.

Table 15: Mean pseudorapidity and width of Gaussian fits to $dE_T/d\eta$.

Reaction	*E_T (GeV)	Mean pseudorapidity	Width
p-Cu	6.9	2.58±0.02	1.25±0.02
	13.7	2.23±0.03	1.16±0.02
	18.3	2.06±0.04	1.09±0.03
	22.9	1.94±0.03	1.03±0.02
	27.4	1.85±0.07	0.99±0.05
	32.0	1.78±0.05	0.94±0.04
	36.6	1.69±0.13	0.92±0.09
	41.1	1.37±0.28	0.98±0.20
p-U	6.9	2.38±0.04	1.36±0.03
	13.7	2.07±0.04	1.23±0.03
	18.3	1.93±0.05	1.15±0.03
	22.9	1.81±0.03	1.06±0.02
	27.4	1.72±0.04	1.01±0.03
	32.0	1.65±0.03	0.95±0.02
	36.6	1.64±0.04	0.86±0.03
	41.1	1.58±0.06	0.81±0.05

*The second column gives the transverse energy at the beginning of the bin.

Figure Captions

Fig. 1 Set-up of HELIOS experiment

Fig. 2 Transverse energy differential cross sections $d\sigma/dE_T$ for $p-D$, $p-Be$, $p-Al$, $p-W$ interactions at 450 GeV/c measured in the backward pseudorapidity region $-0.1 < \eta < 2.9$

Fig. 3 Transverse energy differential cross sections $d\sigma/dE_T$ for $p-A$ interactions at 200 GeV/c.
a) The targets are Be, Al, Cu, W and U, the pseudorapidity coverage is $-0.1 < \eta < 2.9$
b) The targets are Al, Cu, W and U, the pseudorapidity coverage is $-0.1 < \eta < 5.5$

Fig. 4 Distribution of E_T as a function of pseudorapidity in $p-Cu$ and $p-U$ interactions at 200 GeV/c in different E_T slices. The curves are Gaussian fits to the data.

Fig. 5 a) Mean pseudorapidity and b) width as a function of transverse energy in $p-Cu$ and $p-U$ interactions at 200 GeV/c

Fig. 6 Geometrical parametrization of the transverse energy distributions in $p-Al$, $p-Cu$, $p-W$, and $p-U$ interactions at 200 GeV/c

Fig. 7 Comparison between VENUS predictions (histogram) and the experimental $dE_T/d\eta$ distributions (with error bars) for three E_T bins in $p-Cu$ and $p-U$ interactions at 200 GeV/c. The data shown were taken with the trigger condition of at least three charged particles in the acceptance of the Si-counters. This condition was also applied in the simulation, and affects the measured cross section at low E_T not corrected in these distributions.

Fig. 8 Comparison between VENUS predictions (histogram) and the experimental $d\sigma/dE_T$ distributions (with error bars) in $p-Cu$ and $p-U$ interactions at 200 GeV/c. The trigger condition, see Fig. 7, was applied both to data and simulation.

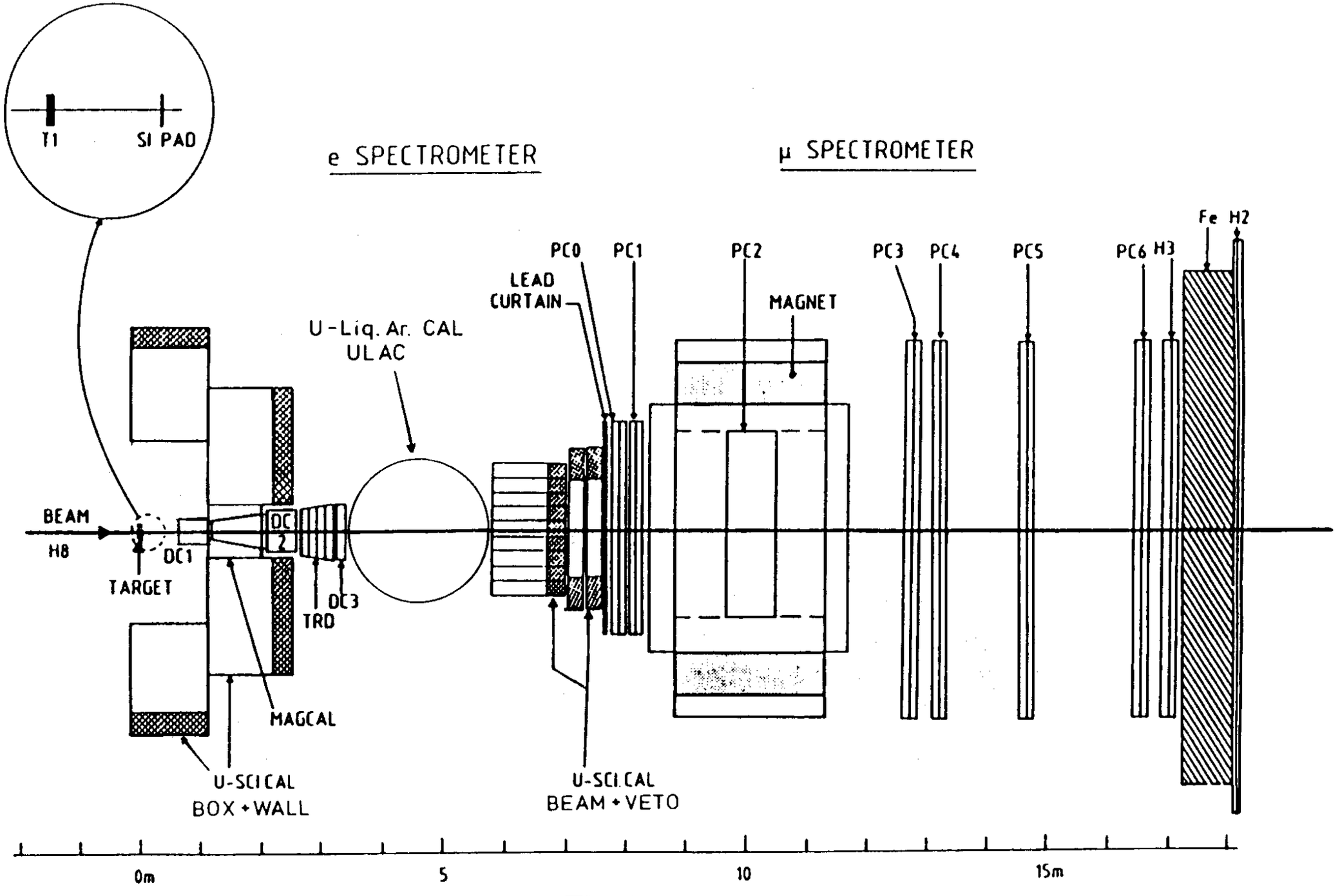
T1
SI PAD
e SPECTROMETER
μ SPECTROMETER
PC0
PC1
PC2
PC3
PC4
PC5
PC6
H3
Fe
H2
LEAD
CURTAIN
MAGNET
U-Liq.Ar. CAL
ULAC
BEAM
H8
DC1
TARGET
DC2
DC3
TRD
MAGCAL
U-SCICAL
BOX+WALL
U-SCICAL
BEAM+VETO
0m
5
10
15m

Fig. 1

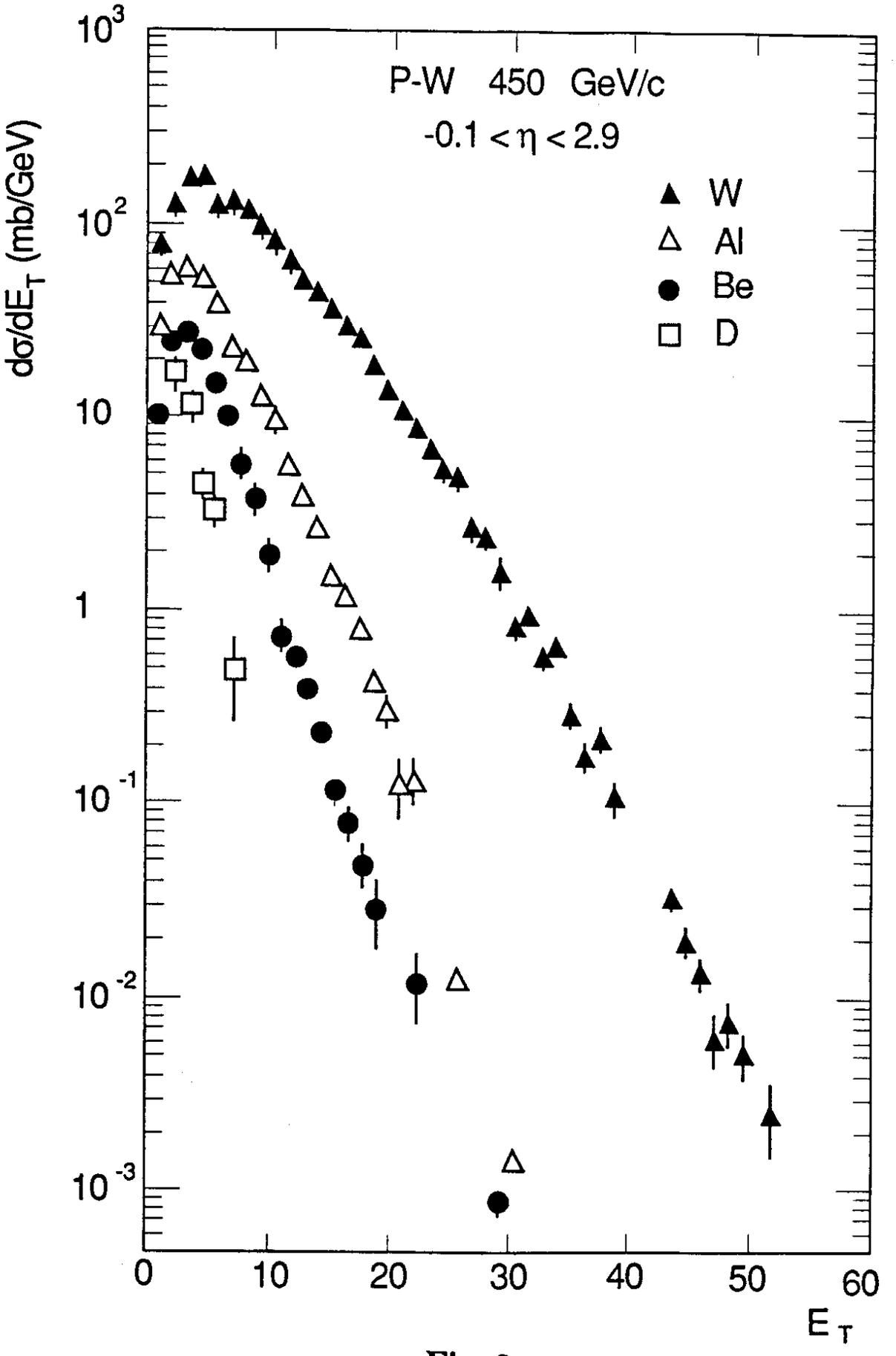
P-W 450 GeV/c
-0.1 < η < 2.9
W
Al
Be
D
dσ/dE_T (mb/GeV)
E_T
10^3
10^2
10
1
10^-1
10^-2
10^-3
0
10
20
30
40
50
60

Fig. 2

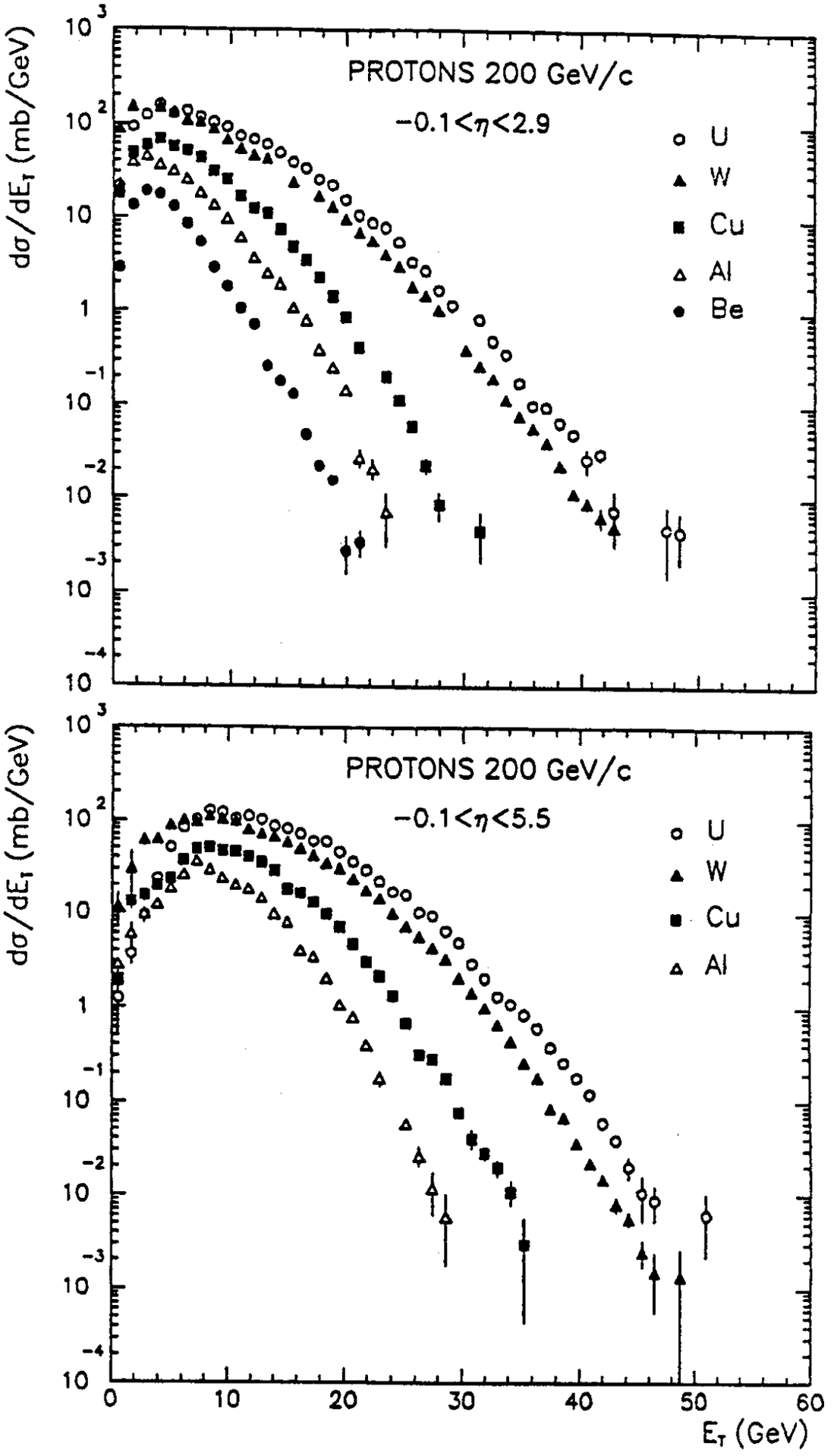
PROTONS 200 GeV/c
−0.1<η<2.9
U
W
Cu
Al
Be
dσ/dE_T (mb/GeV)
PROTONS 200 GeV/c
−0.1<η<5.5
U
W
Cu
Al
dσ/dE_T (mb/GeV)
E_T (GeV)

Fig. 3

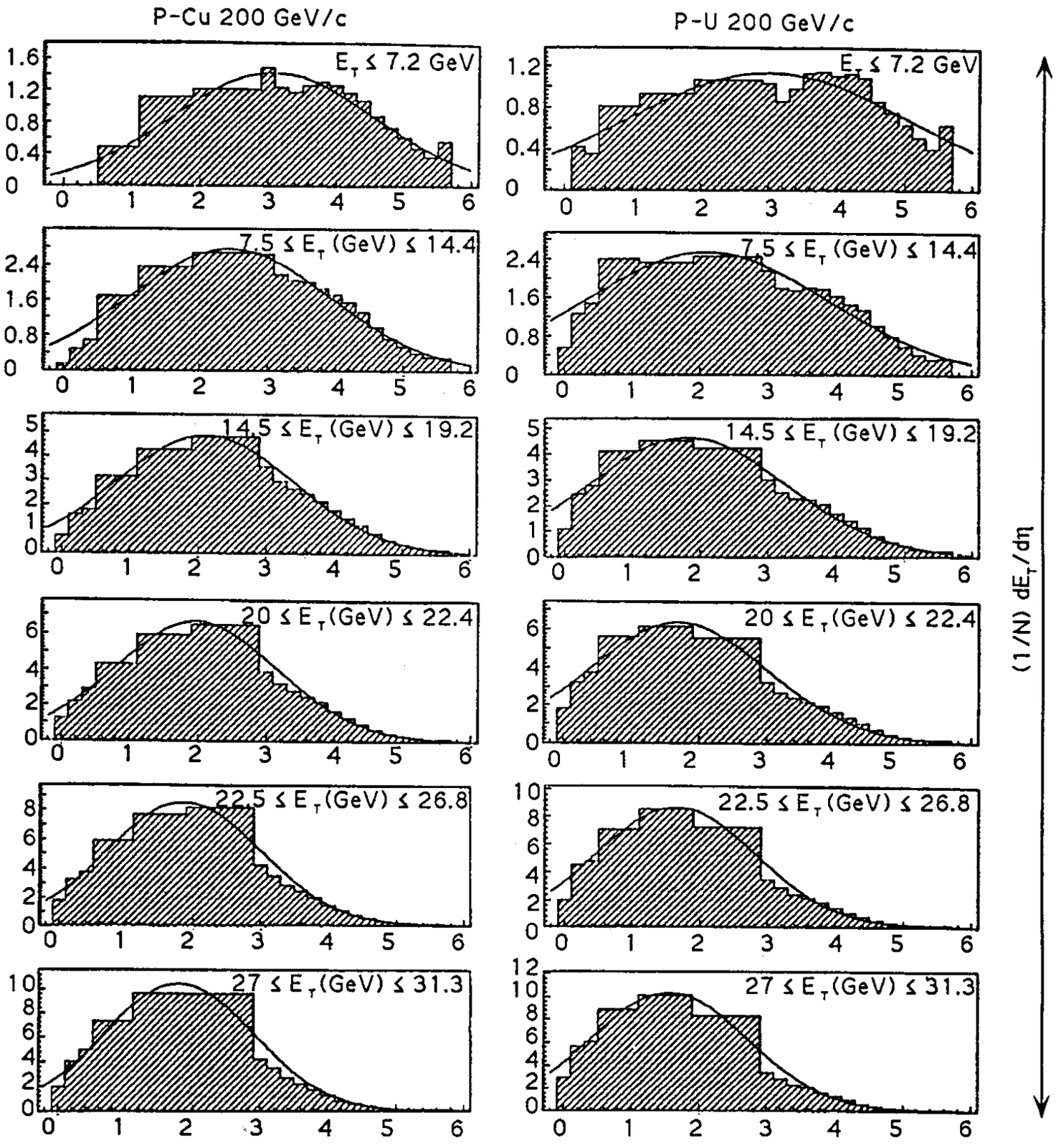
P-Cu 200 GeV/c
P-U 200 GeV/c
$E_T \leq 7.2$ GeV
$7.5 \leq E_T$ (GeV) ≤ 14.4
$14.5 \leq E_T$ (GeV) ≤ 19.2
$20 \leq E_T$ (GeV) ≤ 22.4
$22.5 \leq E_T$ (GeV) ≤ 26.8
$27 \leq E_T$ (GeV) ≤ 31.3
$(1/N)\ dE_T/d\eta$

Fig. 4

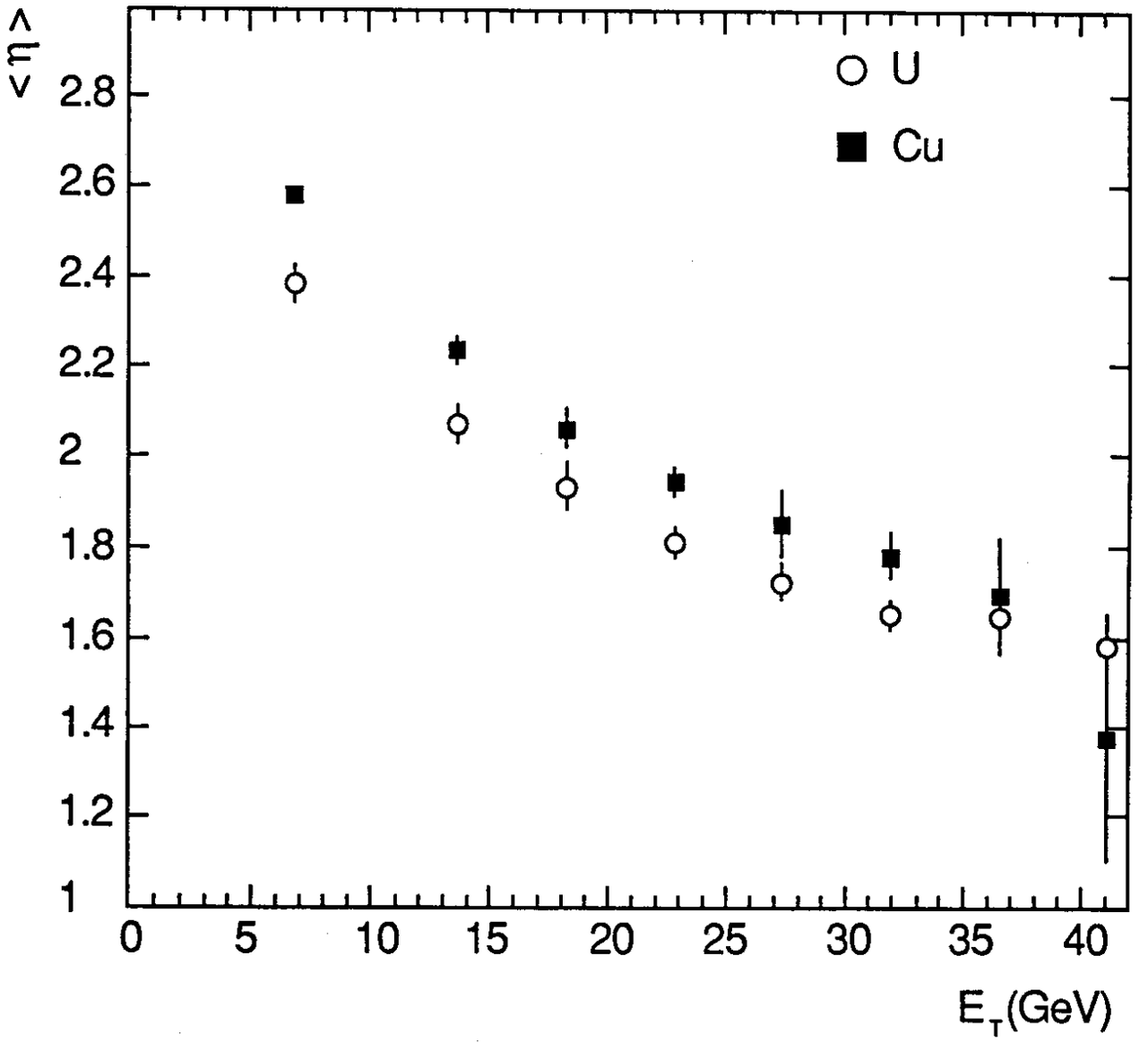
$\langle \eta \rangle$
2.8
2.6
2.4
2.2
2
1.8
1.6
1.4
1.2
1
0
5
10
15
20
25
30
35
40
E_T(GeV)
U
Cu

Fig. 5a

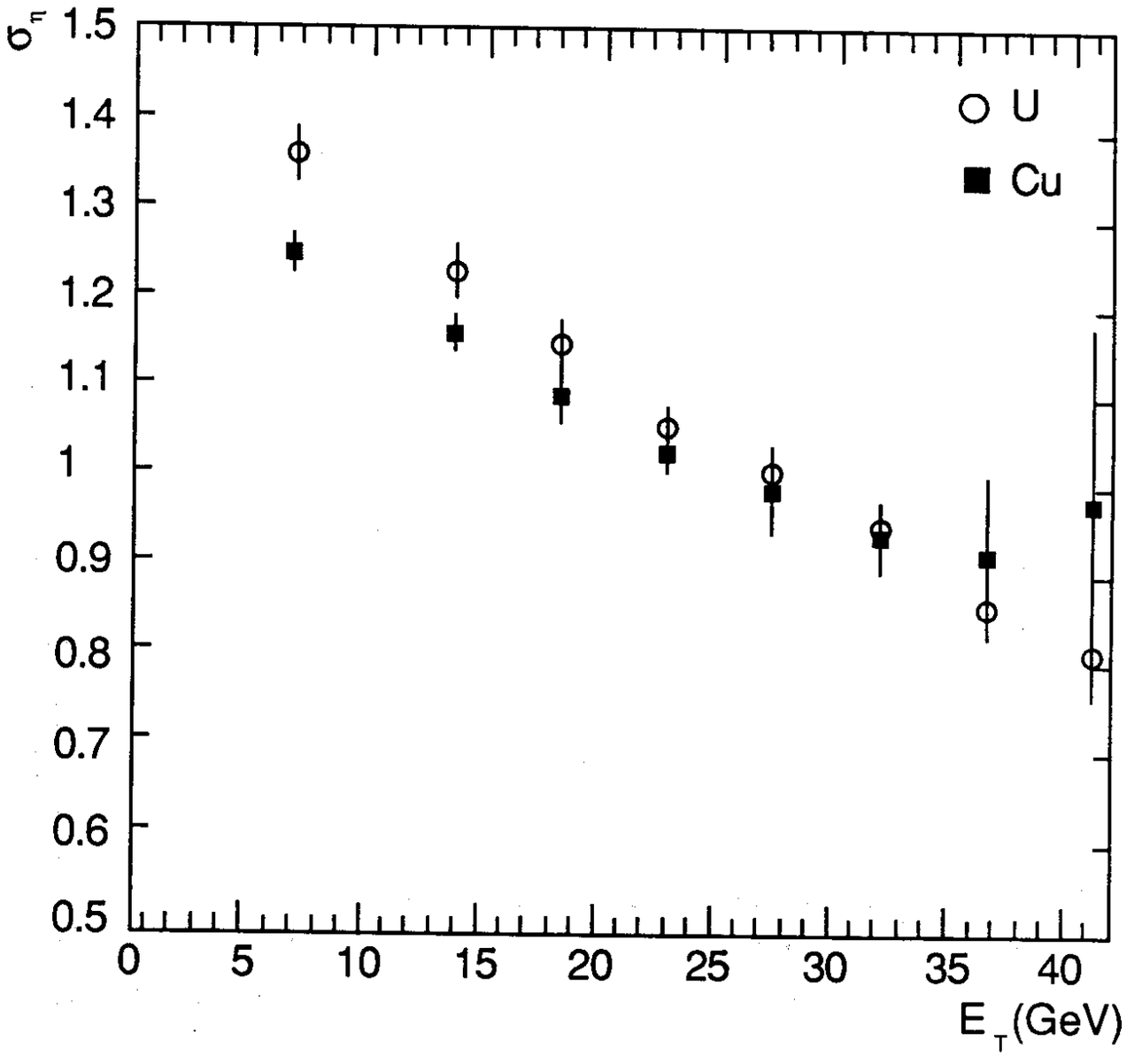

Fig. 5b

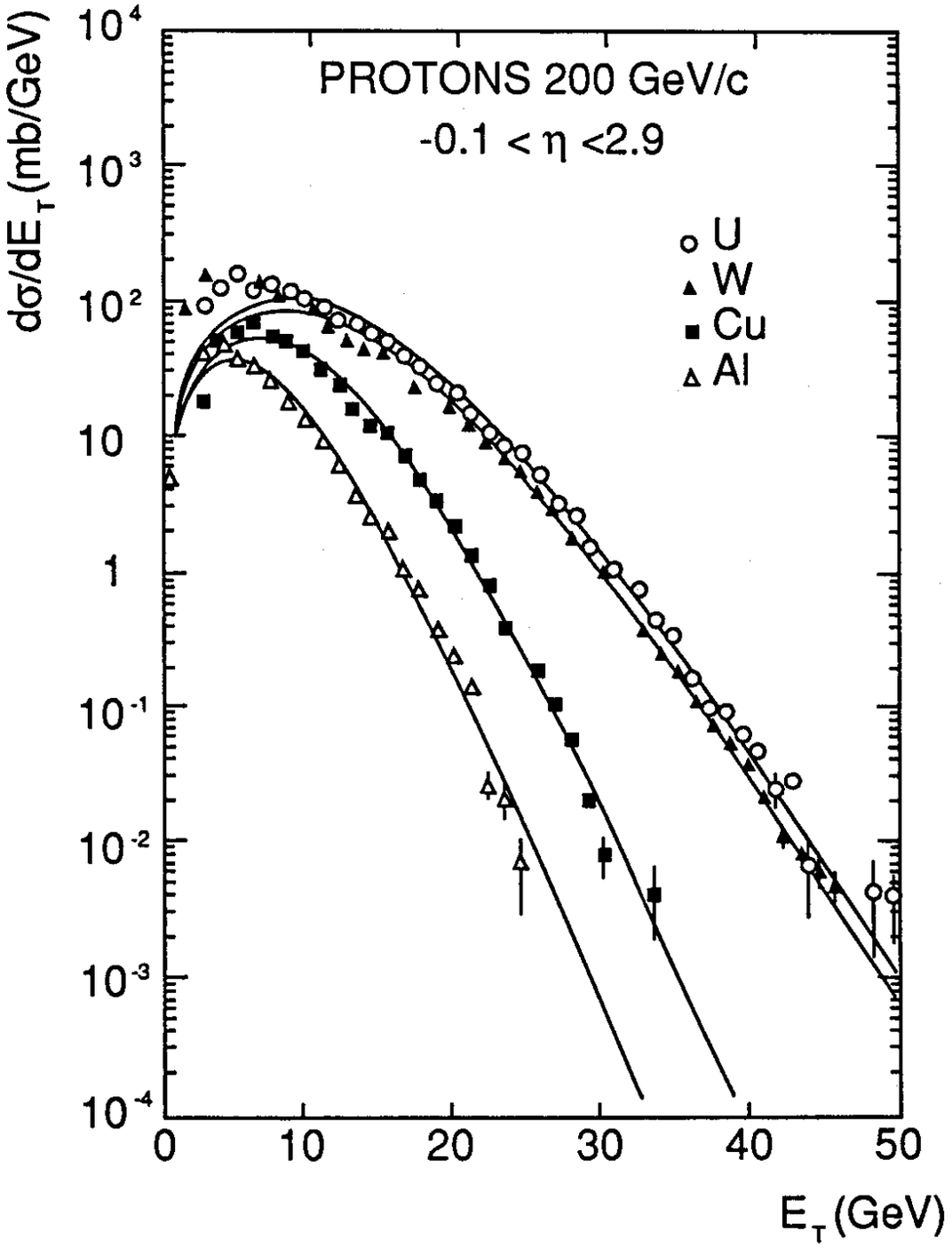
PROTONS 200 GeV/c
-0.1 < η <2.9
U
W
Cu
Al
dσ/dE_T (mb/GeV)
E_T (GeV)
10^4
10^3
10^2
10
1
10^-1
10^-2
10^-3
10^-4
0
10
20
30
40
50

Fig. 6

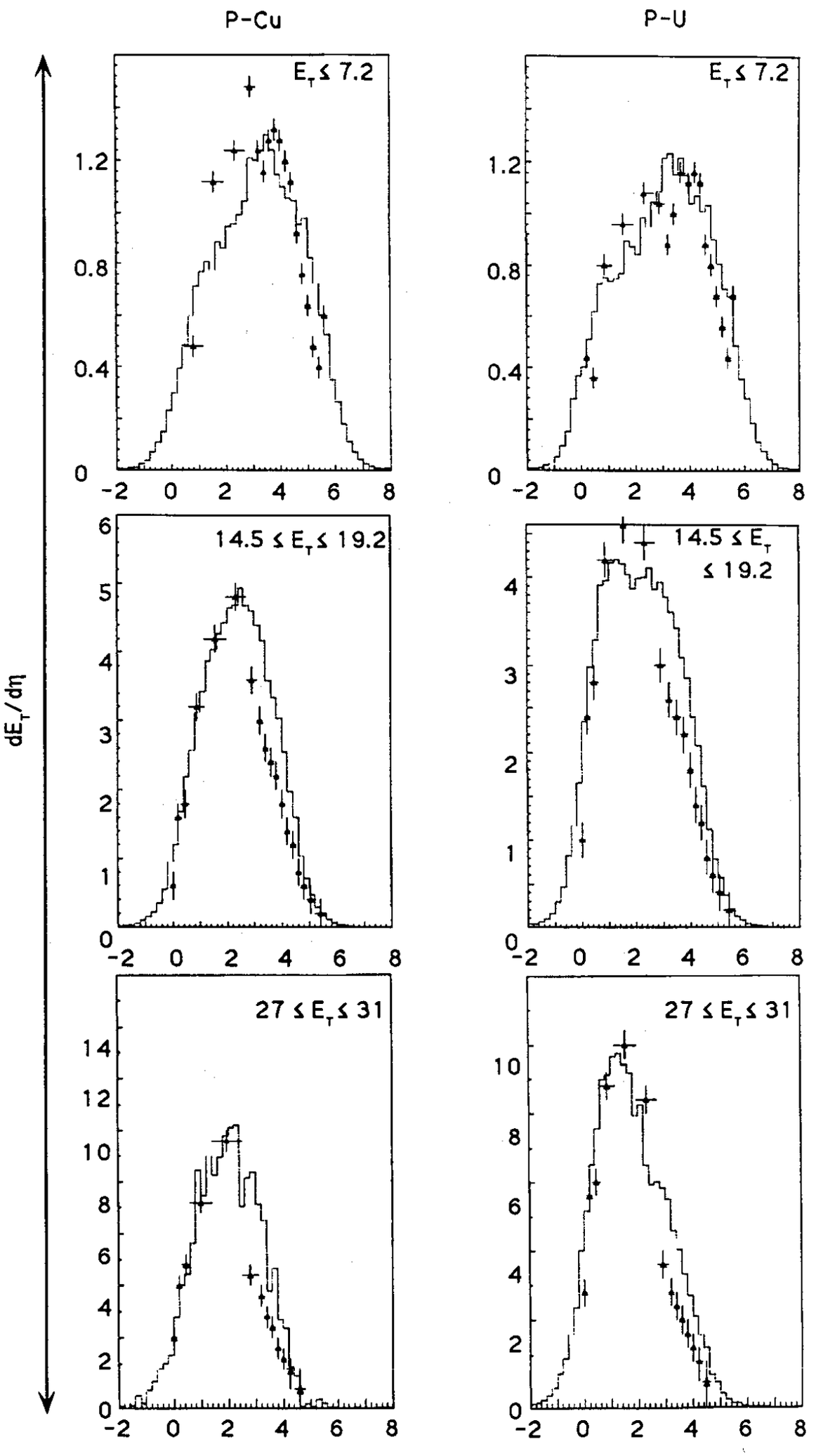

Fig. 7

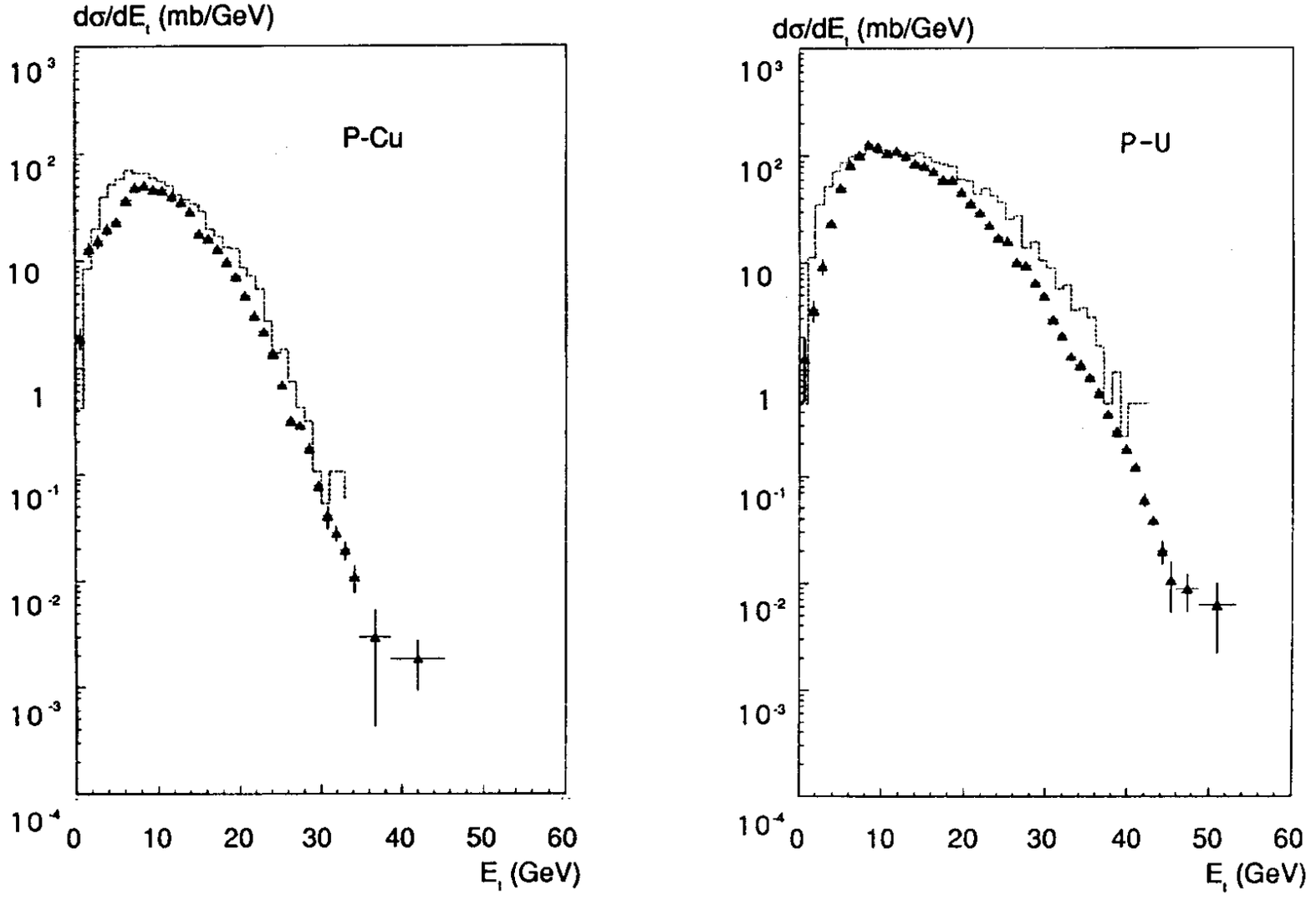
dσ/dE_t (mb/GeV)
P-Cu
10^3
10^2
10
1
10^-1
10^-2
10^-3
10^-4
0
10
20
30
40
50
60
E_t (GeV)
dσ/dE_t (mb/GeV)
P-U
10^3
10^2
10
1
10^-1
10^-2
10^-3
10^-4
0
10
20
30
40
50
60
E_t (GeV)

Fig. 8